

Power transfer efficiency in an air-breathing radio frequency ion thruster

Gao-Huang Huang(黄高煌), Hong Li(李宏), Fei Gao(高飞), and You-Nian Wang(王友年)

Citation: Chin. Phys. B, 2024, 33 (**7**): 075201. DOI: 10.1088/1674-1056/ad426c
Journal homepage: http://cpb.iphy.ac.cn; http://iopscience.iop.org/cpb

What follows is a list of articles you may be interested in

Fundamental study towards a better understanding of low pressure radio-frequency plasmas for industrial applications

Yong-Xin Liu(刘永新), Quan-Zhi Zhang(张权治), Kai Zhao(赵凯), Yu-Ru Zhang(张钰如), Fei Gao(高飞),Yuan-Hong Song(宋远红), and You-Nian Wang(王友年)
Chin. Phys. B, 2022, 31 (**8**): 085202. DOI: 10.1088/1674-1056/ac7551

Numerical investigation of radio-frequency negative hydrogen ion sources by a three-dimensional fluid model

Ying-Jie Wang(王英杰), Jia-Wei Huang(黄佳伟), Quan-Zhi Zhang(张权治), Yu-Ru Zhang(张钰如), Fei Gao(高飞), and You-Nian Wang(王友年)
Chin. Phys. B, 2021, 30 (**9**): 095205. DOI: 10.1088/1674-1056/ac0e21

Time-resolved radial uniformity of pulse-modulated inductively coupled O_2/Ar plasmas

Wei Liu(刘巍), Chan Xue(薛婵), Fei Gao(高飞), Yong-Xin Liu(刘永新), You-Nian Wang(王友年), and Yong-Tao Zhao(赵永涛)
Chin. Phys. B, 2021, 30 (**6**): 065202. DOI: 10.1088/1674-1056/abe3f5

Numerical simulation and experimental validation of multiphysics field coupling mechanisms for a high power ICP wind tunnel

Ming-Hao Yu(喻明浩), Zhe Wang(王哲), Ze-Yang Qiu(邱泽洋), Bo Lv(吕博), and Bo-Rui Zheng(郑博睿)
Chin. Phys. B, 2021, 30 (**6**): 065201. DOI: 10.1088/1674-1056/abeb0e

Quasi-delta negative ions density of Ar/O_2 inductively coupled plasma at very low electronegativity

Shu-Xia Zhao(赵书霞)
Chin. Phys. B, 2021, 30 (**5**): 055201. DOI: 10.1088/1674-1056/abd16a

---

Power transfer efficiency in an air-breathing radio frequency ion thruster

Gao-Huang Huang(黄高煌)[1], Hong Li(李宏)[2,†], Fei Gao(高飞)[1,‡], and You-Nian Wang(王友年)[1]

[1] *Key Laboratory of Materials Modification by Laser, Ion, and Electron Beams (Ministry of Education), School of Physics, Dalian University of Technology, Dalian* 116024, *China*

[2] *College of Physical Science and Technology, Dalian University, Dalian* 116622, *China*

(Received 3 March 2024; revised manuscript received 9 April 2024; accepted manuscript online 24 April 2024)

Due to a series of challenges such as low-orbit maintenance of satellites, the air-breathing electric propulsion has got widespread attention. Commonly, the radio frequency ion thruster is favored by low-orbit missions due to its high specific impulse and efficiency. In this paper, the power transfer efficiency of the radio frequency ion thruster with different gas compositions is studied experimentally, which is obtained by measuring the radio frequency power and current of the antenna coil with and without discharge operation. The results show that increasing the turns of antenna coils can effectively improve the radio frequency power transfer efficiency, which is due to the improvement of Q factor. In pure N_2 discharge, with the increase of radio frequency power, the radio frequency power transfer efficiency first rises rapidly and then exhibits a less steep increasing trend. The radio frequency power transfer efficiency increases with the increase of gas pressure at relatively high power, while declines rapidly at relatively low power. In N_2/O_2 discharge, increasing the N_2 content at high power can improve the radio frequency power transfer efficiency, but the opposite was observed at low power. In order to give a better understanding of these trends, an analytic solution in limit cases is utilized, and a Langmuir probe was employed to measure the electron density. It is found that the evolution of radio frequency power transfer efficiency can be well explained by the variation of plasma resistance, which is related to the electron density and the effective electron collision frequency.

Keywords: radio frequency ion thruster, inductively coupled plasma, power transfer efficiency, analytic solution

PACS: 52.25.Jm, 52.27.Cm, 52.50.Dg **DOI:** 10.1088/1674-1056/ad426c

1. Introduction

In recent years, as the growth of space missions, the environment of low earth orbit (LEO) or lower orbit has attracted worldwide attention of scientists. There are many advantages in reducing the orbital height. For instance, the optical imaging system carried on the earth observation satellite can obtain higher spatial resolution, and the signal-to-noise ratio of the radar system in the communication satellite can be improved.[1] Additional benefit include lessen orbital debris, cheaper cost of satellite launch, etc. One of successful examples is the European Space Agency's gravity field and steady-state ocean circulation explorer (GOCE) which has operated stably for 4.5 years at an altitude of 260 km–229 km.[2]

However, reducing the orbital height will strengthen the atmospheric drag, and then affect the long-term orbit maintenance of spacecraft. To overcome this difficulty, scientists have proposed to use air-breathing electric propulsion (ABEP) technology below 250 km.[3–5] ABEP is a cross innovation of efficient gas collecting technology and electric propulsion technology, which is commonly composed of an intake device and a thruster. It aims to carry no propellant and provides long-life thrust for low orbit spacecraft by absorbing the orbital rarefied atmosphere as propellant.

Nevertheless, the atmospheric gas is usually hard to ignite or discharge due to its low ionization rate.[6,7] Kozhevnikov *et al.*[8] pointed out that radio frequency ion thruster (RIT) can be an appropriate selection used at certain altitudes with low thrust demand due to its high specific impulse and efficiency. For example, RIT-10 was used to send Artemis to the scheduled orbit for almost one year after the Ariane-5 rocket was broken down.[9] In addition, RIT exhibits distinct advantages compared to other types of electric propulsion technology, such as Hall thrusters. The structure of RIT is simple and easy to miniaturize, allowing for the design of various sizes to meet the thrust requirements of different space missions.[10] Moreover, RIT has a long lifespan and performs well at low powers, which can be attributed to its excellent combination of electrodeless discharge, high control accuracy, fast response, and homogeneous beam.[11,12]

The ionization chamber of RIT is an inductively coupled plasma (ICP) source with cylindrical geometry, in which electromagnetic field accelerates free electrons to break down neutral gas to generate the plasma. As the RF power varies, ICP usually exhibits two distinct regimes, the so-called E (electrostatic) mode at low RF power for capacitive coupling and the H (electromagnetic) mode at high RF power for inductive

†Corresponding author. E-mail: lihong10@dlu.edu.cn
‡Corresponding author. E-mail: fgao@dlut.edu.cn

© 2024 Chinese Physical Society and IOP Publishing Ltd

coupling.[13–15] In the H mode, the maintenance of plasma is dominated by angular electric field, while it mainly dominates by axial electric field generated by electric potential difference between both ends of the coil in the E mode. Since the plasma density are much higher in the H mode in comparison with that in the E mode,[16,17] it is necessary to keep RIT operating in the H mode.

In general, the absorbed power of plasma is inevitably less than the output power of the power supply, which is due to the power loss when the current passes through the matching network, transmission line, antenna coil, and the interface. In order to reduce this power loss and improve the ionization rate, it is necessary to improve the plasma absorption power, or RF power transfer efficiency. For RF driven ICP, the plasma power absorption is closely related to the electron heating mechanism. It is known that, at high pressures, the electron heating mechanism is typically dominated by Ohmic heating, while at low pressures, the stochastic heating plays a leading role.[18–20]

At present, the relevant research on the RF power transfer efficiency of the ICP source is mainly concentrated in the fields of neutral beam injection,[21–23] material processing,[24] etc., but very few in the application of RIT. Chabert *et al.*[25] evaluated the RF power transfer efficiency of an RIT with Xe as propellant using a global model. They found that the RF power transfer efficiency decreases from 82% to 34% with the increase of RF power, and rises first rapidly then slower to about 80% with the increase of gas mass flow. Zheng *et al.*[26] simulated an ICP source with an inner radius of 18.5 mm and a length of 180 mm with O and N_2 as propellants based on COMSOL Multiphysics. The results show that the RF power transfer efficiency is only 10%–30%, which declines slightly with the increase of RF power, and rises with the increase of propellant mass flow rate. Under the same input conditions, the RF power transfer efficiency of oxygen atoms discharge is higher than that of nitrogen molecules discharge. Lopez-Uricoechea *et al.*[27] studied an RIT with a driven frequency of 13.56 MHz, a radius of 2.54 cm and a length of 25.4 cm using the global model. The results show that the ionization rate and electron temperature decrease with the increase of the mass flow rate, resulting in inversely proportional relationship between the discharge efficiency and the gas mass utilization efficiency. Masillo *et al.*[28] investigated the effect of applying an external magnetic field on inductive plasma thruster (IPT) with simulations (ADAMANT and HELIC code) and experimental measurements (based on IPG-6S). The results show that the plasma resistance and RF power absorbed by plasma can be enhanced with an externally applied DC magnetic field within some intensity limits. Herdrich *et al.*[29] successfully applied the MHD effect to maximize plasma power in an inductively driven plasma wind tunnel PWK3. The results show that increasing the mass flow rate can increase the total efficiency at high anode voltages for oxygen plasma.

The above research is mainly based on simulations and few experiments, which lacks systematically experimental support, not considering the impact of external circuit. In addition, in conventional research of thruster, the vacuum chamber pressure is only a function of gas flow.[30,31] However, in the ABEP, the pressure depends on the compression ratio of the intake device,[32] the collecting efficiency, the intake area, and the orbital atmospheric density at different altitudes. Therefore, it is necessary to investigate the influence of pressure on RF power transfer efficiency under the condition of fixed gas flow.

In order to better understand the power absorption mechanism of RIT and improve the RF power transfer efficiency, we systematically studied the effects of antenna coil turns, discharge power, gas pressure, and gas composition on the RF power transfer efficiency of RIT by means of experiment. One of the main diagnostic tools is a single Langmuir probe, which is used to diagnose plasma parameters (electron density) under different operating conditions. Besides, the analytic solutions of plasma resistance in the limit case of different electron densities and pressures are discussed to give a better understanding of the evolutionary trend of RF power transfer efficiency under various conditions.

The structure of the article is arranged as follows: Section 2 introduces the experimental device, diagnostic method, and analytic solutions. Section 3 discusses the experimental results, corresponding to the effects of antenna coil turns, RF power, gas pressure, and gas composition on the RF power transfer efficiency. Section 4 is a brief summary.

2. Experimental setup, diagnostics, and analytic solutions

2.1. Experimental setup

In this paper, the RIT source consists of an ionization chamber, a double layer grid, and an expansion chamber, as shown in Fig. 1. The ionization chamber is a quartz tube with a wall thickness of 5 mm, an inner radius of 3 cm, a height of 10 cm, and a hole in radius of 1.5 cm at the top of the tube. A cylindrical spiral antenna coil with different turns is wrapped around the tube, and the coil is supported by insulating material to ensure the same space between each turn. The antenna coil is made of hollow copper wire with an outer diameter of 4 mm, an inner diameter of 2 mm, and a spacing distance of 5 mm between each turn. One side of the coil is connected to an RF power supply with a frequency of 13.56 MHz and a maximum power of 500 W through a matching network, and the other side is grounded. The gas enters the ionization chamber through the stainless-steel head fixed on the top of

the quartz tube, and the mass flow rate is fixed at 5 sccm by a mass flowmeter. A grounded shield is installed outside the quartz tube to prevent RF leakage. The expansion chamber is made of stainless steel with a radius of 10.5 cm and a height of 18 cm. Connecting the ionization chamber and expansion chamber is a screen grid and an acceleration grid, and each grid has 151 holes with a diameter of 1 mm.

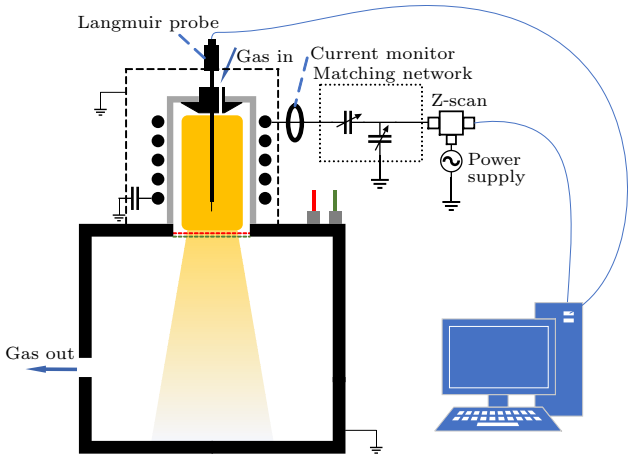


Fig. 1. Schematic diagram of RIT source and diagnostic systems.

2.2. Experimental diagnostics

A Z-scan is placed between the matching network and the power supply to monitor the forward power and reflected power. The RF current passing through the antenna coil is obtained by a current monitor (Pearson^{TM}, Model 4997) installed between the antenna coil and the matching network. A single Langmuir probe (Impedans ALP System^{TM}) is used to measure the electron density. The probe tip is made of tungsten wire or platinum wire with a diameter of 0.3 mm and a length of 5 mm. It is inserted from the top of the quartz tube and is fixed at the center of the ionization chamber and 1 cm above the screen grid. An RF filter unit is placed between the probe holder and the data acquisition module to address the RF interference. Moreover, in order to reduce capacitive coupling, a ceramic capacitor is inserted between the antenna coil and the ground.[33–35] When ignoring the resistance component, the voltage of the capacitor between the antenna coil and the ground presents a phase difference of 180° from the voltage of the coil itself. By adjusting the capacitor to an appropriate value ($L_c C\omega^2 = 2$), there is a voltage node (a virtual ground point) in the center of the coil. Thus, for the same current in the coil, the voltage at both ends of the coil is half that in the absence of a capacitor. Reducing the capacitive component can alleviate the plasma potential fluctuations, resulting in more accurate Langmuir single probe measurements. Finally, both grids are grounded to serve as a reference for the probe potential.[36,37]

The RF power transfer efficiency is the ratio of plasma absorbed power to the output power of RF generator, and can be obtained experimentally by the following formula:

$$\zeta = \frac{P_{\rm abs}}{P_{\rm a}} = \frac{P_{\rm a} - I_{\rm rms}^2 R}{P_{\rm a}}, \tag{1}$$

where $P_{\rm abs}$ is the plasma absorbed power, $P_{\rm a}$ is the applied power which represents the output power without reflected power of RF generator, $I_{\rm rms}$ is the root-mean-square (RMS) current through antenna coil, and R is the equivalent circuit resistance obtained without discharge.

2.3. Electromagnetic model and analytic solutions

RF power transfer efficiency can also be obtained by an electromagnetic model. More details of the electromagnetic model and analytic solutions can be found in the book by Chabert and Braithwaite.[38]

Since the length of the ionization chamber is much larger than the radius, it is reasonable to consider only the z-direction magnetic field $\tilde{H}_z$ and the angular electric field $\tilde{E}_\theta$. And, the electromagnetic field related with the inner radius r can be obtained by solving Maxwell's equations

$$\tilde{H}_z = H_{z0} \frac{\mathrm{J}_0(kr)}{\mathrm{J}_0(kr_0)}, \tag{2a}$$

$$\tilde{E}_\theta = -\frac{\mathrm{i}kH_{z0}}{\omega\varepsilon_0\varepsilon_{\rm p}} \frac{\mathrm{J}_1(kr)}{\mathrm{J}_0(kr_0)}, \tag{2b}$$

where H_{z0} is the magnetic field at the radial boundary. J_0 is the zero-order Bessel function and J_1 is the first-order Bessel function. $k = k_0\sqrt{\varepsilon_{\rm p}}$ is the complex wavenumber in the plasma, in which k_0 is the wavenumber in the vacuum and $\varepsilon_{\rm p}$ is the plasma dielectric constant related to the electron density and effective electron collision frequency. ε_0 is the vacuum dielectric constant, ω is the angular driven frequency and i is the imaginary unit.

According to the complex Poynting theorem, neglecting the displacement current in the dielectric layer and assuming $\tilde{H}_z(r = r_{\rm c}) = H_{z0}$, we can obtain the complex power input $\tilde{P}$ of the cylindrical ICP system and subsequently the plasma resistance $R_{\rm ind}$, which is equal to the real part of $Z_{\rm ind}$, indicating the plasma absorption power.

$$\tilde{P} = -\frac{1}{2}\tilde{E}_\theta(r_{\rm c})\tilde{H}_z(r_{\rm c})(2\pi r_{\rm c} l) = \frac{1}{2} Z_{\rm ind} I_{\rm coil}^2, \tag{3a}$$

$$R_{\rm ind} = \frac{2\mathrm{Re}\left(\tilde{P}\right)}{I_{\rm coil}^2} = \frac{2\pi N_{\rm c}^2}{l\omega\varepsilon_0} \mathrm{Re}\left[\frac{\mathrm{i}kr_0\mathrm{J}_1(kr_0)}{\varepsilon_{\rm p}\mathrm{J}_0(kr_0)}\right], \tag{3b}$$

where $r_{\rm c}$ is the outer radius of the ionization chamber, l is the length of the ionization chamber, $Z_{\rm ind}$ is the total complex impedance of the system, $I_{\rm coil}$ is the RF current flowing through the antenna coil ($I_{\rm coil} = \sqrt{2} I_{\rm rms}$), and $N_{\rm c}$ is the antenna coil turns.

As such, RF power transfer efficiency can be expressed as a function of the plasma resistance as follows:

$$\zeta = \frac{P_{\rm abs}}{P_{\rm abs} + P_{\rm coil}} = \left[1 + \frac{R}{R_{\rm ind}}\right]^{-1}, \tag{4a}$$

$$\frac{R}{R_{\rm ind}} = k_0 r_0 \left(\frac{2r_{\rm c}^2}{Qr_0^2}\right)\left\{4{\rm Re}\left[\frac{{\rm i}{\rm J}_1(kr_0)}{\sqrt{\varepsilon_{\rm p}}{\rm J}_0(kr_0)}\right]\right\}, \quad (4b)$$

where $P_{\rm abs}$ is the absorbed power by plasma, i.e., $P_{\rm abs} = \frac{1}{2}R_{\rm ind}I_{\rm coil}^2$, and $P_{\rm coil}$ is the power dissipated in the antenna coils, i.e., $P_{\rm coil} = \frac{1}{2}RI_{\rm coil}^2$. Q is the quality factor of the coils. It can be seen that the power transfer efficiency is positively correlated with the plasma resistivity $R_{\rm ind}$.

In order to give a better understanding of physical mechanism of the power transfer efficiency, the analytic solutions of plasma resistance in the limit cases of different density and pressure are discussed. At low electron density case, the electron-plasma frequency $\omega_{\rm pe} = (e^2 n_{\rm e}/(\varepsilon m_{\rm e}))^{1/2}$ is comparable with the effective electron collision frequency $\nu_{\rm eff}$ and ω. The angular electric field $\tilde{E}_\theta$ can be expressed as $\tilde{E}_\theta = -(\mu_0 r/(2l)){\rm i}\omega N_{\rm c} I_{\rm coil}$, according to the Faraday's law. In a range of low pressures, $\nu_{\rm eff} \ll \omega$, then the plasma permittivity satisfies $\varepsilon_{\rm p} \approx -\omega_{\rm pe}^2/\omega^2$, and the current density $\tilde{J}_\theta$ can be expressed as $\tilde{J}_\theta = {\rm i}\omega\varepsilon_0\varepsilon_{\rm p}\tilde{E}_\theta$. This allows the absorbed power to be given as

$$\begin{aligned} P_{\rm abs} &\approx \int_0^{2\pi}\int_0^{r_0}\int_0^{l}\frac{\left|\tilde{J}_\theta\right|^2}{2\sigma_{\rm dc}} r{\rm d}\phi\,{\rm d}r{\rm d}z \\ &\approx \frac{n_{\rm e}e^2\nu_{\rm eff}\mu_0^2\pi r_0^4}{4m_{\rm e}l}N_{\rm c}^2 I_{\rm coil}^2. \end{aligned} \quad (5)$$

Then the plasma resistance is

$$R_{\rm ind} \approx \frac{n_{\rm e}e^2\nu_{\rm eff}\mu_0^2\pi r_0^4 N_{\rm c}^2}{2m_{\rm e}l}, \quad (6)$$

where $n_{\rm e}$ is the electron density, e is the elementary charge, μ_0 is the permeability of vacuum, $m_{\rm e}$ is the electron mass, and $\sigma_{dc} = (e^2 n_{\rm e}/(m_{\rm e}\nu_{\rm eff}))$ is the direct current conductivity. It can be seen that $R_{\rm ind}$ increases with increasing gas pressures ($\nu_{\rm eff}$) and electron density.

However, at high pressures, $\varepsilon_{\rm p} \approx -\omega_{\rm pe}^2/({\rm i}\omega\nu_{\rm eff})$, the plasma resistance is

$$R_{\rm ind} \approx \frac{n_{\rm e}e^2\omega^2\mu_0^2\pi r_0^4 N_{\rm c}^2}{2m_{\rm e}l\nu_{\rm eff}}. \quad (7)$$

It can be seen that $R_{\rm ind}$ increases with increasing electron density, while it decreases with gas pressures.

On the other hand, at high electron density case and in the limit of low pressures, the electron-plasma frequency and effective electron-collision frequency satisfy $\omega_{\rm pe} \gg \omega \gg \nu_{\rm eff}$, such that $\varepsilon_{\rm p} \approx 1 - \omega_{\rm pe}^2(1 + {\rm i}\nu_{\rm eff}/\omega)/\omega^2$. Then the wave number in plasma can be written as

$$k = k_0\sqrt{\varepsilon_{\rm p}} \approx {\rm i}k_0\frac{\omega_{\rm pe}}{\omega}\left(1 + \frac{{\rm i}\nu_{\rm eff}}{2\omega}\right), \quad (8)$$

which gives $|kr_0| \gg 1$. As a result,

$${\rm i}{\rm J}_1(kr_0) \approx \frac{-1}{\sqrt{kr_0}}{\rm e}^{kr_0}, \quad {\rm J}_0(kr_0) \approx \frac{1}{\sqrt{kr_0}}{\rm e}^{kr_0}. \quad (9)$$

According to Eq. (3b) and ${\rm Re}\left[-1/\sqrt{\varepsilon_{\rm p}}\right] \approx \nu_{\rm eff}/(2\omega_{\rm pe})$, we can obtain

$$R_{\rm ind} \approx \frac{2\pi k_0 r_0 N_{\rm c}^2}{l\omega\varepsilon_0}{\rm Re}\left[\frac{-1}{\sqrt{\varepsilon_{\rm p}}}\right] \approx \frac{\pi r_0\nu_{\rm eff}N_{\rm c}^2}{lc\varepsilon_0\omega_{\rm pe}}, \quad (10)$$

which shows that $R_{\rm ind}$ is directly proportional to gas pressures, and inversely proportional to the square root of electron density.

Table 1. A list of plasma variables.

Symbol	Quantity
c	vacuum light speed
e	elementary charge
μ_0	vacuum permeability
ε_0	vacuum dielectric constant
ω	angular driven frequency
k_0	vacuum wavenumber
l	height of the ionization chamber
$r_{\rm c}$	outer radius of ionization chamber
r_0	inter radius of ionization chamber
H_{z0}	magnetic field at the radial boundary
${\rm J}_0$	zero-order Bessel function
${\rm J}_1$	first-order Bessel function
$n_{\rm g}$	neutral gas density
$n_{\rm e}$	electron density
$N_{\rm c}$	antenna coil turns
Q	quality factor
ζ	RF power transfer efficiency
$\tilde{P}$	complex input power
$P_{\rm abs}$	absorbed power by plasma
$P_{\rm a}$	applied power
$P_{\rm coil}$	dissipated power by coils
$I_{\rm rms}$	root mean square current
$I_{\rm coil}$	amplitude of antenna coil current
R	equivalent circuit resistance
Q	quality factor
$Z_{\rm ind}$	total complex impedance
$R_{\rm ind}$	plasma resistance
$\tilde{H}_z$	z-direction magnetic field
$\tilde{E}_\theta$	angular electric field
$\varepsilon_{\rm p}$	plasma dielectric constant
$\omega_{\rm pe}$	electron-plasma frequency
k	complex wavenumber in the plasma
$\nu_{\rm eff}$	effective electron collision frequency
$\nu_{\rm m}$	electron-neutral momentum transfer collision frequency
$\nu_{\rm stoc}$	stochastic collision frequency
$K_{\rm el}$	elastic collision rate coefficients
$\delta_{\rm eff}$	anomalous skin depth
$\bar{v}_{\rm e}$	electron mean velocity
$L_{\rm c}$	coil inductance

In the limit of high pressures, $\omega_{\rm pe} \gg \nu_{\rm eff} \gg \omega$, the plasma permittivity satisfies $\sqrt{\varepsilon_{\rm p}} \approx \frac{\omega_{\rm pe}}{\sqrt{2\nu_{\rm eff}\omega}}(1+{\rm i})$. Based on the asymptotic behavior of the Bessel function at imaginary arguments, the plasma resistance is

$$R_{\rm ind} \approx \frac{\pi r_0 N_{\rm c}^2}{lc\varepsilon_0\omega_{\rm pe}}\sqrt{2\nu_{\rm eff}\omega}, \quad (11)$$

which shows that $R_{\rm ind}$ is directly proportional to the square root of the effective electron collision frequency, and inversely proportional to square root of electron density.

It should be noted that $\nu_{\rm eff}$ is the effective electron collision frequency considered both the Ohmic heating and the stochastic heating, which can be estimated by the following formula:[39]

$$\nu_{\rm eff} = \nu_{\rm m} + \nu_{\rm stoc}, \tag{12a}$$

$$\nu_{\rm m} = n_{\rm g} K_{\rm el}, \tag{12b}$$

$$\nu_{\rm stoc} \approx \frac{\bar{\upsilon}_{\rm e}}{4\delta_{\rm eff}}, \tag{12c}$$

$$\delta_{\rm eff} \approx \left(\frac{\overline{\upsilon_{\rm e}} c^2}{\omega \omega_{\rm pe}^2} \right)^{1/3}, \tag{12d}$$

where $\nu_{\rm m}$ is the electron–neutral momentum transfer collision frequency, $\nu_{\rm stoc}$ is the stochastic collision frequency, $n_{\rm g}$ is the neutral gas density, and $K_{\rm el}$ is the elastic collision rate coefficients. $\delta_{\rm eff}$ is the anomalous skin depth, $\bar{\upsilon}_{\rm e} = \sqrt{8k_{\rm B}T_{\rm e}/(\pi m)}$ is the electron mean velocity, and c is the speed of light in the vacuum. All variables presented above are summarized in Table 1 for clarity.

3. Results and discussion

With respect to the inductively coupled nitrogen and nitrogen–oxygen plasma applied to low-orbit thrusters, the influence of antenna coil turns, RF power, gas pressure, and gas composition on RF power transfer efficiency is discussed. Furthermore, at various operating conditions, the plasma parameters (i.e., the electron density and effective electron collision frequency) are presented to explain the evolution of RF power transfer efficiency.

3.1. The influence of coil turns, RF power, and gas pressure

In the experiment, we measured the equivalent circuit resistance R for different antenna coil turns $N_{\rm c} = 3, 5, 7$ by linear fitting the data obtained without discharge. More details of the measurement can be found in Ref. [40]. As shown in Fig. 2(a), the R increases monotonously from 0.61 Ω to 1.48 Ω with increasing $N_{\rm c}$ from 3 to 7 turns. Furthermore, the quality factor of coils $Q = \omega L_{\rm c}/R$ is calculated by the actual measurement of the coil inductance $L_{\rm c}$ and the equivalent circuit resistance R, as shown in Fig. 2(b). Here, the coil inductance is measured using a vector network analyzer at 13.56 MHz, and the equivalent circuit resistance is used to consider both the coils and the matching network dissipation.[41] It can be seen that the $L_{\rm c}$ and Q factor rise monotonically with increasing $N_{\rm c}$.

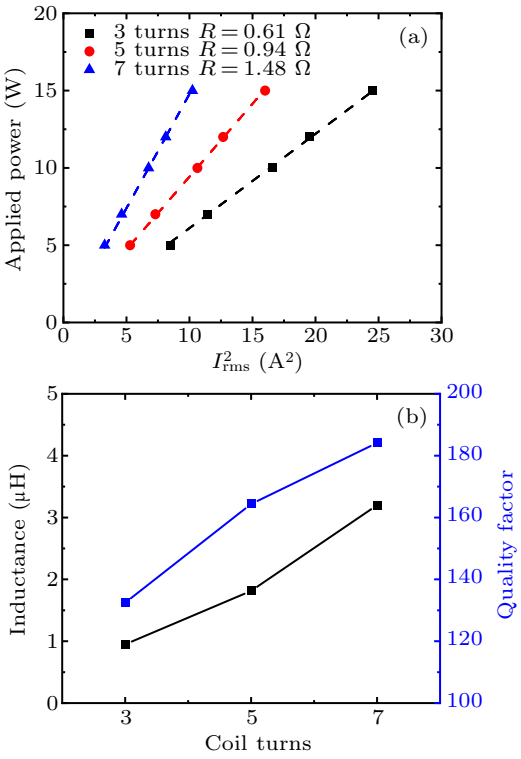


Fig. 2. (a) The equivalent resistance of the circuit operated without discharge operation, (b) the measured inductance of antenna coils and the corresponding quality factor Q for different $N_{\rm c}$.

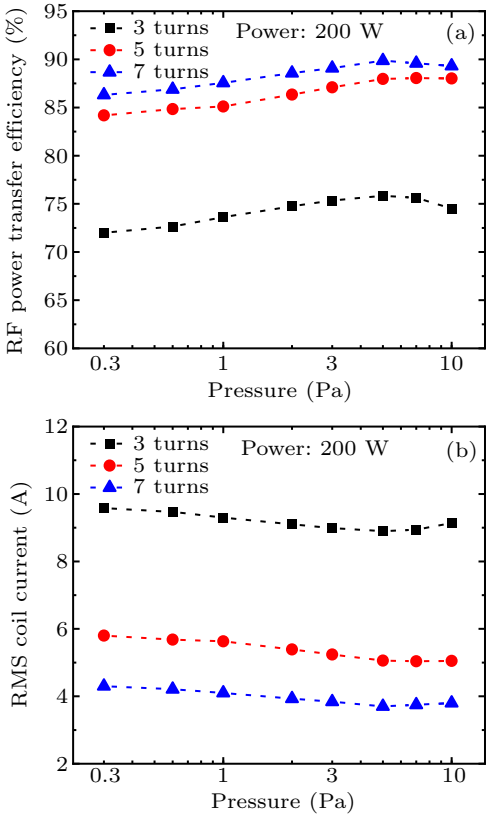


Fig. 3. (a) RF power transfer efficiency and (b) RMS coil current versus gas pressure (0.3 Pa–10 Pa) for different $N_{\rm c}$ at 200 W with N_2 discharge.

Figure 3 shows the tendency of RF power transfer efficiency ζ and RMS coil current versus gas pressure varying from 0.3 Pa to 10 Pa for different $N_{\rm c}$ at 200 W with N_2 discharge. From Fig. 3(a), it can be seen that when $N_{\rm c}$ changes

from 3 to 5 turns, ζ increases considerably in the entire pressure range, e.g., it increases by about 11.5% at 1 Pa and 200 W. This increase of ζ can be attributed to the enhancement of Q factor caused by the increase of the coil inductance, according to Eq. (4). It can also be reflected from Fig. 3(b), in which the current decreases by about 4 A when N_c varies from 3 to 5 turns. And then, the remarkable drop of the current effectively reduces the Ohmic loss through the circuit loop, though R increases by about 0.33 Ω. However, when N_c varies from 5 to 7 turns, ζ increases slightly, e.g., it rises by only 2.4% at 1 Pa and 200 W. From Fig. 3(b), we can also see that, the current decreases by less than 2 A, but R rises by about 0.54 Ω. The combined effect leads to an insignificant reduction in the Ohmic loss of the circuit. Indeed, when the number of coil turns is beyond a certain number, the self-resonance frequency of the coil could be close to the driving frequency, and it may adversely affect the Q factor of the coil.[42]

Figure 4 shows the RF power transfer efficiency ζ, the electron density, and the ionization degree as a function of gas pressure varying from 0.3 Pa to 10 Pa for different RF powers (100 W–300 W) at $N_c = 3$ turns with N_2 discharge. As shown in Fig. 4(a), with the increase of RF power from 100 W to 300 W, ζ first rises rapidly and then increases at a slower rate in the whole pressure range. In addition, when the gas pressure varies from 0.3 Pa to 10 Pa, the evolution of ζ with gas pressure demonstrates diversity for different RF powers. For instance, when the RF power is fixed at 100 W, with the increase of gas pressure, ζ is almost unchanged in the pressure range of 0.3 Pa–2 Pa, while it drops dramatically in the pressure range of 3 Pa–10 Pa. When the RF power is fixed at 300 W, ζ rises rapidly in the pressure range of 0.3 Pa–5 Pa and rises at a slower rate in the pressure range of 5 Pa–10 Pa. It can be seen that the position where ζ starts to fall gradually moves towards higher gas pressure with the increase of RF power.

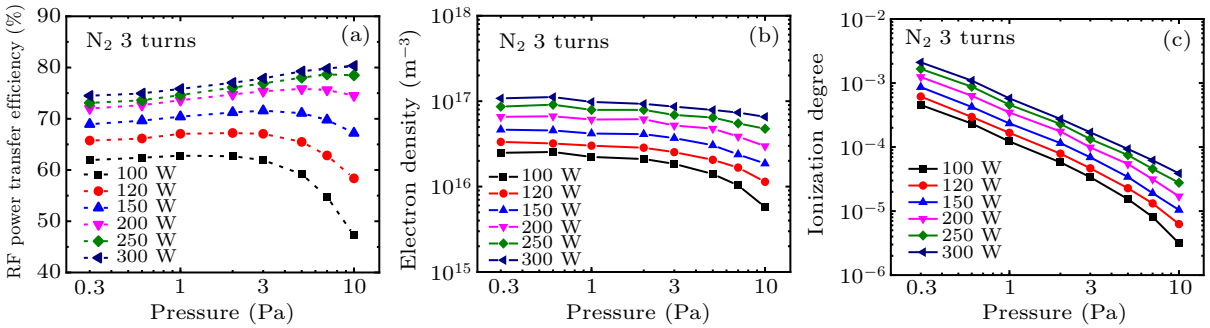


Fig. 4. (a) RF power transfer efficiency, (b) electron density, and (c) ionization degree versus gas pressure (0.3 Pa–10 Pa) for different RF powers at $N_c = 3$ turns with N_2 discharge.

These trends mentioned above can be explained by the analytic solutions of the plasma resistance R_{ind} in the limit cases according to Eqs. (6), (7), (10), and (11), which is related to the electron density n_e and the effective electron collision frequency ν_{eff}. As shown in Fig. 4(b), the electron density decreases monotonically with increasing gas pressure, and especially it declines rapidly from 5 Pa to 10 Pa at low RF power. With respect to the evolution of the RF power transfer efficiency at 100 W, corresponding to the low-density case, R_{ind} increases linearly both with n_e and ν_{eff} at low pressure, as given in Eq. (6). The inverse effect of n_e and ν_{eff} finally results in an almost unchanged ζ with gas pressure. At high pressure, R_{ind} is directly proportional to n_e and inversely proportional to ν_{eff}, as given in Eq. (7). The combined effect contributes to a sharp decline of RF power transfer efficiency. Similarly, the trend of RF power transfer efficiency at 300 W can also be revealed, which is corresponding to the high-density case. At low pressure, R_{ind} is inversely proportional to the square root of n_e and is directly proportional to ν_{eff}, as presented in Eq. (10), resulting in a rapid climb of ζ. At high pressure, R_{ind} is inversely proportional to the square root of n_e and is directly proportional to the square root of ν_{eff}, as shown in Eq. (11), accounting for a slower increase of ζ.

Considering the importance of ion in the electric propulsion system used for extracting, the ionization degree is also calculated by the ratio of the electron density to the total density of electron and neutral gas, assuming a neutral gas temperature of $T_g = 0.17 \times P_{abs} + 387$ K.[43] As shown in Fig. 4(c), it can be seen that the degree of ionization reaches its maximum value above 10^{-3} at 0.3 Pa and 300 W, then it decreases monotonously with increasing gas pressure due to the combined effect of the slow decline of electron density and the monotonical increase of neutral gas density.

3.2. The influence of gas composition

The particle number density at different orbital altitudes is obtained using the NRLMSISE-00 model,[44] in which the solar activity is assumed to be mean and the input parameters are solar flux $F_{10.7} = 140$ and geomagnetic index $A_p = 15$, as shown in Fig. 5. It can be seen that the atmospheric compositions are mainly O, O_2, and N_2 at 150 km–250 km. Here, we assume that the atomic oxygen is recombined after collecting by the intake device.[27,45,46] The ratio of N_2 and O_2 (N_2/O_2) can be calculated, where the O_2 density is equal to

the O_2 density plus half of the O density. The N_2 content in N_2/O_2 discharge is set as 38%, 56%, and 72% in experiment, corresponding to altitudes of 250 km, 200 km, and 150 km, respectively.

Figure 6(a) shows the ζ varying with gas pressure for O_2 discharge at different RF powers, and the similar trend is observed as that of N_2. Figures 6(b) and 6(c) show the ζ as a function of gas pressure for different N_2 contents in N_2/O_2 discharge at 100 W and 300 W, respectively. From Fig. 6(b), it can be seen that ζ decreases slightly with increasing N_2 content at low pressures (0.3 Pa–3 Pa). As the gas pressure and N_2 content further increases, the ζ shows a sharply downward trend. For example, ζ decreases by about 8% with the N_2 content increases from 0% to 38% at 10 Pa. From Fig. 6(c), it can be seen that ζ increases monotonically with increasing gas pressure and N_2 content at 300 W. Similarly, investigating the variation of electron density and effective electron collision frequency under the corresponding operating conditions can be helpful to understand these trends of RF power transfer efficiency.

Figure 7 shows the measured electron density varying with gas pressure for different N_2 contents at 100 W and 300 W in N_2/O_2 discharge. It can be seen that the electron density shows a downward trend with increasing of N_2 content both at 100 W and 300 W. This is because the ionization collision cross section of N_2 is smaller than that of O_2,[48] and accordingly the ionization energy of O_2 ($\varepsilon_{i,O} = 12.07$ eV, $\varepsilon_{i,N} = 15.58$ eV) is lower, so more electrons can be generated through the ionization reaction with O_2.

The effective electron collision frequency ν_{eff} as a function of gas pressure for different N_2 contents at 100 W and 300 W in N_2/O_2 discharge is also estimated by calculating elastic collision rate coefficients of N_2 and O_2 based on data from Refs. [43,49], according to Eq. (12), as shown in Fig. 8.

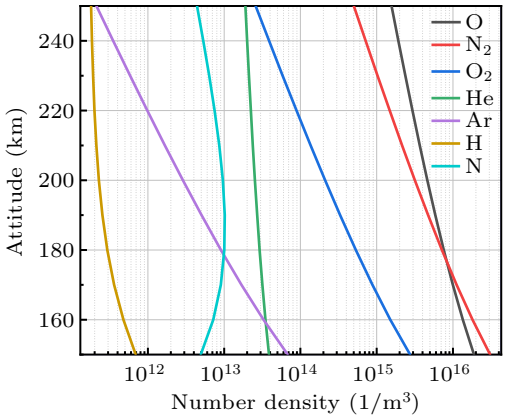


Fig. 5. Particle number density varying with orbital height of 150 km–250 km for different species at the mean solar activity.[47]

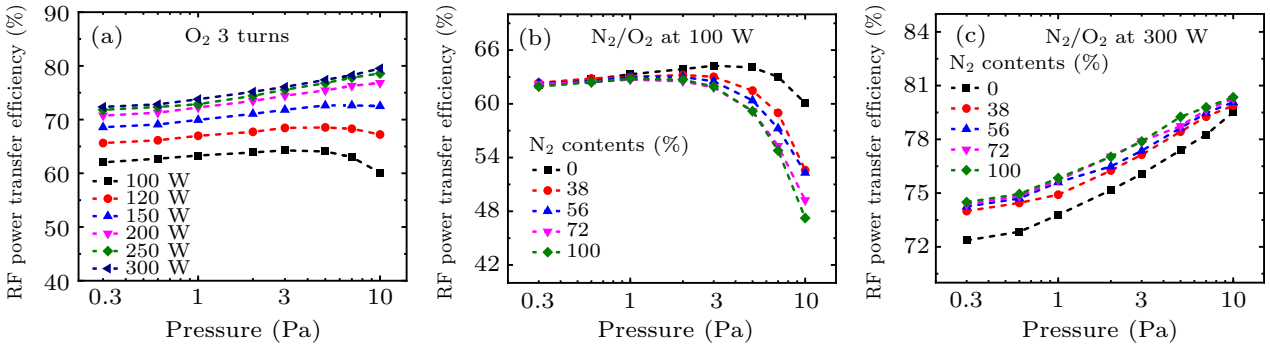


Fig. 6. RF power transfer efficiency varying with gas pressure for (a) different RF powers in O_2 discharge; (b) different N_2 contents in N_2/O_2 discharge at 100 W, and (c) different N_2 contents in N_2/O_2 discharge at 300 W.

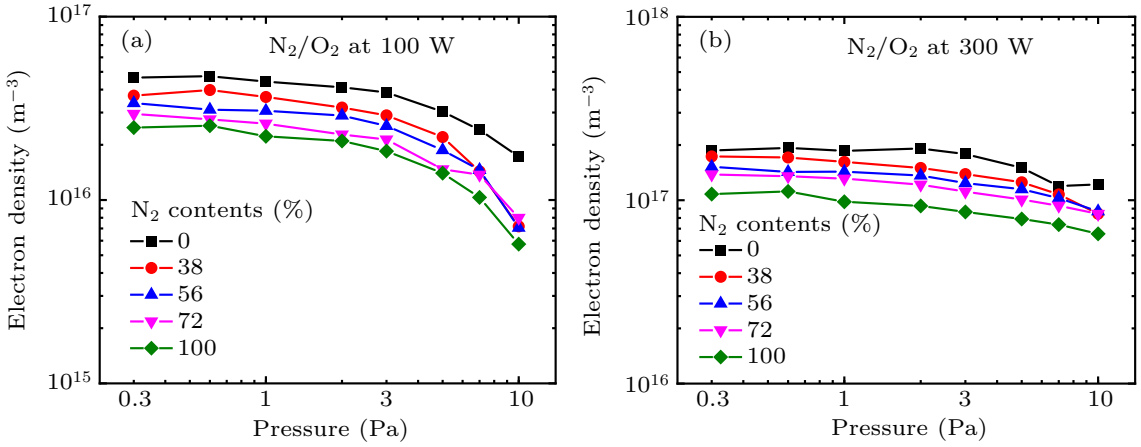


Fig. 7. The measured electron density varying with gas pressure for different N_2 contents at (a) 100 W and (b) 300 W in N_2/O_2 discharge.

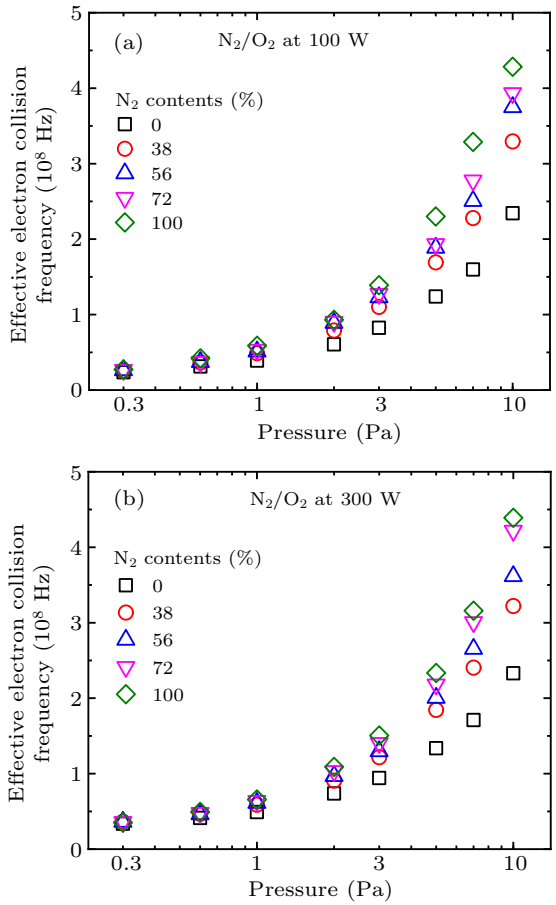


Fig. 8. The calculated effective electron collision frequency varying with gas pressure for different N_2 contents at (a) 100 W and (b) 300 W in N_2/O_2 discharge.

It can be seen that $\nu_{\rm eff}$ increases monotonically with increasing gas pressure just as expected.[50] However, the evolution of $\nu_{\rm eff}$ with N_2 content demonstrates diversity at low and high pressures both for 100 W and 300 W. It increases slightly with increasing N_2 content at low gas pressures (i.e., 0.3 Pa–3 Pa), while $\nu_{\rm eff}$ increases significantly with the increase of N_2 content at high gas pressures (i.e., 5 Pa–10 Pa). These trends can be contributed to the relevant electron heating mechanisms. It is known that the stochastic heating of electrons is important at low pressures (i.e., $\nu_{\rm stoc}$ is comparable to $\nu_{\rm m}$), while Ohmic heating dominates at higher pressures (i.e., $\nu_{\rm m} \gg \nu_{\rm stoc}$).[18,19] At low pressures, the drop of electron density with increasing N_2 content leads to a slight decrease of $\nu_{\rm stoc}$ ($\nu_{\rm stoc} \propto n_{\rm e}^{1/3}$), according to Eqs. (12c) and (12d). Nevertheless, since the elastic collision cross section of N_2 is greater than that of O_2,[48] increasing N_2 content could lead to a remarkable increase of $\nu_{\rm m}$. At last, the combined effect contributes to the slight rise of $\nu_{\rm eff}$ with increasing N_2 content. At high pressures, $\nu_{\rm m}$ is more important, thus increasing the N_2 content can result in the increase of ν_m and $\nu_{\rm eff}$, according to Eq. (12b).

With respect to the evolution of ζ with N_2 content at 100 W, corresponding to the low-density case, $R_{\rm ind}$ increases linearly with $n_{\rm e}$, as given in Eqs. (6) and (7). At low pressure, $R_{\rm ind}$ increases linearly with $\nu_{\rm eff}$. Consequently, both the rapid drop of electron density and the slow rise of $\nu_{\rm eff}$ result in the slight decline of ζ with increasing N_2 content. At high pressure, $R_{\rm ind}$ is inversely proportional to $\nu_{\rm eff}$. Thus, the rapid drop of electron density combined with the remarkable increase of $\nu_{\rm eff}$ leads to a sharp decline of ζ, as shown in Fig. 6(b).

As to the evolution of ζ with N_2 content at 300 W, corresponding to the high-density case, $R_{\rm ind}$ is inversely proportional to the square root of $n_{\rm e}$, as given in Eqs. (10) and (11). At low pressure, $R_{\rm ind}$ increases linearly with $\nu_{\rm eff}$. Therefore, the rapid drop of electron density and the slight rise of $\nu_{\rm eff}$ result in the increase of ζ with increasing N_2 content. At high pressure, $R_{\rm ind}$ increases with the square root of $\nu_{\rm eff}$. Thus, the rapid drop of electron density combined with the significant increase of $\nu_{\rm eff}$ determines the increase of ζ, as shown in Fig. 6(c).

4. Conclusion

In summary, the effects of antenna coil turn $N_{\rm c}$, RF power, gas pressure, and gas composition on the radio frequency power transfer efficiency ζ and power absorption mechanism in an RF ion thruster were investigated using a Langmuir probe, Z-scan, and current probe. It is found that increasing $N_{\rm c}$ from 3 to 5 turns could dramatically increase the ζ due to the increase of Q factor.

In pure N_2 discharge, with the increase of RF power, the ζ first rises and then exhibits a slower increasing rate. With the increase of gas pressure, the ζ rises monotonically at high power, while it is almost unchanged first and then decreases sharply at low power. In N_2/O_2 discharge, the N_2 content is varied to investigate the effect of gas composition based on the actual orbital environment. It is found that increasing the N_2 content can lead to an increase of ζ at high RF power, while it results in a decrease of ζ at low RF power.

These trends of ζ can be well understood by analyzing the evolution of $R_{\rm ind}$ varied with $n_{\rm e}$ and $\nu_{\rm eff}$ in limit cases. The results obtained in this work may provide a better understanding of the underlying power absorption mechanism in the air-breathing radio frequency ion thruster, which is helpful to further optimize the source design and improve the RF power transfer efficiency.

Acknowledgements

Project supported by the National Natural Science Foundation of China (Grant Nos. 12005031 and 12275041) and the Natural Science Fund from the Interdisciplinary Project of Dalian University (Grant No. DLUXK-2023-QN-001). The atmospheric data have been provided by the Community Coordinated Modeling Center (CCMC) at Goddard Space Flight Center through their publicly available simulation services

(https://ccmc.gsfc.nasa.gov). The NRLMSISE-00 Model was developed by J. M. Picone, A. E. Hedin, and D. P. Drob at the Naval Research Laboratory.

References

[1] Crisp N H, Roberts P C E, Livadiotti S, Oiko V T A, Edmondson S, Haigh S J, Huyton C, Sinpetru L A, Smith K L, Worrall S D, Becedas J, Domínguez R M, González D, Hanessian V, Mølgaard A, Nielsen J, Bisgaard M, Chan Y A, Fasoulas S, Herdrich G H, Romano F, Traub C, García-Almiñana D, Rodríguez-Donaire S, Sureda M, Kataria D, Outlaw R, Belkouchi B, Conte A, Perez J S, Villain R, Heißerer B and Schwalber A 2020 *Prog. Aeronaut. Sci.* **117** 100619

[2] Steiger C, Romanazzo M, Emanuelli P P, Floberghagen R and Fehringer M 2014 *Proceedings of the 13rd International Conference on Space Operations*, May 5–9, 2014, Pasadena, USA, p. 1934

[3] Di Cara D, Gonzalez del Amo J, Santovincenzo A, Carnicero Domíguez B, Arcioni M, Caldwell A and Roma I 2007 *Proceedings of the 30th International Electric Propulsion Conference*, September 17–20, 2007, Florence, Italy, Vol. 21 p. 22

[4] Schonherr T, Komurasaki K, Romano F, Massuti-Ballester B and Herdrich G 2015 *IEEE Trans. Plasma Sci.* **43** 287

[5] Tisaev M, Ferrato E, Giannetti V, Paissoni C, Baresi N, Lucca Fabris A and Andreussi T 2022 *Acta Astronaut.* **191** 374

[6] Cifali G, Misuri T, Rossetti P, Andrenucci M, Valentian D and Feili D 2011 *Proceedings of the 47th AIAA/ASME/SAE/ASEE Joint Propulsion Conference*, July 31–August 03, 2011, San Diego, USA, p. 6073

[7] Andreussi T, Ferrato E, Giannetti V, Piragino A, Paissoni C A, Cifali G and Andrenucci M 2019 *Proceedings of the AIAA Propulsion and Energy* 2019 *Forum*, August 19–22, 2019, Indianapolis, USA, p. 3995

[8] Kozhevnikov V V, Smirnov P E, Suvorov M O and Khartov S A 2017 *Therm. Eng.* **64** 952

[9] Killinger R, Kukies R, Surauer M, Tomasetto A and van Holtz L 2003 *Acta Astronaut.* **53** 607

[10] Groh K H and Loebtt H W 1991 *J. Propul. Power* **7** 573

[11] Bathgate S N, Bilek M M M and Mckenzie D R 2017 *Plasma Sci. Technol.* **19** 083001

[12] Li Y H, Chen Y C, Liu S W and Aslan A R 2023 *Acta Astronaut.* **208** 130

[13] Lee H C, Kim D H and Chung C W 2013 *Appl. Phys. Lett.* **102** 234104

[14] Daltrini A M, Moshkalev S A, Morgan T J, Piejak R B and Graham W G 2008 *Appl. Phys. Lett.* **92** 061504

[15] Gao F, Li X C, Zhao S X and Wang Y N 2012 *Chin. Phys. B* **21** 075203

[16] Ostrikov K N, Xu S and Yu M Y 2000 *J. Appl. Phys.* **88** 2268

[17] Liu W, Gao F, Zhao S X, Li X C and Wang Y N 2013 *Phys. Plasmas* **20** 123513

[18] Tyshetskiy Y O, Smolyakov A I and Godyak V A 2002 *Plasma Sources Sci. Technol.* **11** 203

[19] Godyak V A and Kolobov V I 1998 *Phys. Rev. Lett.* **81** 369

[20] Godyak V A, Piejak R B, Alexandrovich B M and Kolobov V I 1998 *Phys. Rev. Lett.* **80** 3264

[21] Li H, Gao F, Wen D Q, Yang W, Du P C and Wang Y N 2019 *J. Appl. Phys.* **125** 173303

[22] Jain P, Recchia M, Cavenago M, Fantz U, Gaio E, Kraus W, Maistrello A and Veltri P 2018 *Plasma Phys. Contr. Fusion* **60** 045007

[23] Zielke D, Briefi S and Fantz U 2021 *J. Phys. D: Appl. Phys.* **54** 155202

[24] Kralkina E A, Rukhadze A A, Pavlov V B, Vavilin K V, Nekliudova P A, Petrov A K and Alexandrov A F 2016 *Plasma Sources Sci. Technol.* **25** 015016

[25] Chabert P, Arancibia Monreal J, Bredin J, Popelier L and Aanesland A 2012 *Phys. Plasmas* **19** 073512

[26] Zheng P, Wu J, Zhang Y, Che B and Li J 2021 *Acta Astronaut.* **187** 236

[27] Lopez-Uricoechea J, Lev D and Walker M L R 2022 *J. Electr. Propuls.* **1** 11

[28] Masillo S, Romano F, Soglia R, Herdrich G, Roberts P, Schönherr T, Binder T, Boxberger A, Traub C, Fasoulas S, Smith K, Edmondson S, Haigh S, Crisp N, Toshiyuki V, Oiko V, Lyons R, Worrall S, Livadiotti S and Pavarin D 2018 *Proceedings of the 7th Russian-German Conference on Electric Propulsions*, October 21–26, 2018, Rauischholzhausen, German

[29] Herdrich G and Petkow D 2008 *J. Plasma Phys.* **74** 391

[30] Dietz P, Gärtner W, Koch Q, Köhler P E, Teng Y, Schreiner P R, Holste K and Klar P J 2019 *Plasma Sources Sci. Technol.* **28** 084001

[31] Schmidt J, Laufer R, Hyde T and Herdrich G 2020 *Vacuum* **176** 109338

[32] Wu J, Zheng P, Zhang Y and Tang H 2022 *Prog. Aerosp. Sci.* **133** 100848

[33] Suzuki K, Konishi K, Nakamura K and Sugai H 2000 *Plasma Sources Sci. Technol.* **9** 199

[34] Han D, Lee H C, Kim H J, Kim Y S, Chung C W and Chae H 2013 *Plasma Sources Sci. Technol.* **22** 055011

[35] Kim T W, Kim J H, Lee M Y and Chung C W 2020 *Phys. Plasmas* **27** 073505

[36] Chen F F 2001 *Phys. Plasmas* **8** 3029

[37] Godyak V A, Piejak R B and Alexandrovich B M 2002 *Plasma Sources Sci. Technol.* **11** 525

[38] Chabert P and Braithwaite N 2011 *Physics of Radio-Frequency Plasmas,* (Cambridge: Cambridge University Press)

[39] Lieberman M A and Lichtenberg A J 2005 *Principles of Plasma Discharges and Materials Processing*, 2nd edn. (New York: Wiley)

[40] Hopwood J 1994 *Plasma Sources Sci. Technol.* **3** 460

[41] Godyak V A, Piejak R B and Alexandrovich B M 1999 *J. Appl. Phys.* **85** 703

[42] Godyak V A and Alexandrovich B M 2017 *Rev. Sci. Instrum.* **88** 083512

[43] Thorsteinsson E G and Gudmundsson J T 2009 *Plasma Sources Sci. Technol.* **18** 045001

[44] Picone J M, Hedin A E, Drob D P and Aikin A C 2002 *J. Geophys. Res.* **107** SIA 15

[45] Li Y, Chen X, Li D, Xiao Y, Dai P and Gong C 2015 *Vacuum* **120** 89

[46] Tagawa M, Yokota K, Nishiyama K, Kuninaka H, Yoshizawa Y, Yamamoto D and Tsuboi T 2013 *J. Propul. Power* **29** 501

[47] NRLMSISE-00 Atmosphere Model, 2023 https://kauai.ccmc.gsfc.nasa.gov/instantrun/nrlmsis/

[48] LXCat, Plasma Data Exchange Project, 2023, https://nl.lxcat.net/

[49] Thorsteinsson E G and Gudmundsson J T 2010 *Plasma Sources Sci. Technol.* **19** 055008

[50] Du P C, Zhao M L, Li H, Gao F and Wang Y N 2022 *J. Appl. Phys.* **131** 133301